



HAL
open science

Synthesis of cerium oxide-based nanostructures in near- and supercritical fluids

Cédric Slostowski, Samuel Marre, Jean-Marc. Bassat, Cyril Aymonier

► **To cite this version:**

Cédric Slostowski, Samuel Marre, Jean-Marc. Bassat, Cyril Aymonier. Synthesis of cerium oxide-based nanostructures in near- and supercritical fluids. *Journal of Supercritical Fluids*, 2013, 84, pp.89-97. 10.1016/j.supflu.2013.09.014 . hal-00877938

HAL Id: hal-00877938

<https://hal.science/hal-00877938>

Submitted on 1 Jul 2022

HAL is a multi-disciplinary open access archive for the deposit and dissemination of scientific research documents, whether they are published or not. The documents may come from teaching and research institutions in France or abroad, or from public or private research centers.

L'archive ouverte pluridisciplinaire **HAL**, est destinée au dépôt et à la diffusion de documents scientifiques de niveau recherche, publiés ou non, émanant des établissements d'enseignement et de recherche français ou étrangers, des laboratoires publics ou privés.

Synthesis of cerium oxide-based nanostructures in near- and supercritical fluids

Cédric Slostowski^{ab} Samuel Marre^{ab} Jean-Marc Bassat^{ab} Cyril Aymonier^{ab}

^a CNRS, ICMCB, UPR9048, F-33600 Pessac, France

^b Université de Bordeaux, ICMCB, UPR9048, F-33600 Pessac, France

Abstract :

Cerium-oxide based nanostructures attract increasing interest for their use in multiple applications. In particular, the substitution of Ce atoms by other elements with lower oxidation state is used to control oxygen vacancies within the oxide structures, which can greatly enhance the material properties for catalysis applications. Among the synthesis approaches, supercritical water (scH₂O) has been proved to be an extremely efficient media for the fast and facile elaboration of pure CeO₂ nanostructures, although substitution was little investigated with this method (precursors' reactivity, mechanisms, etc.). Here, the influence of two cerium precursors – Ce(NO₃)₃·6H₂O and Ce(NO₃)₆(NH₄)₂ – in scH₂O synthesis was first investigated over the CeO₂ nanostructures synthesis process. Cerium ammonium nitrate was later used as precursor for the synthesis of Ce_{1-x-y}A_xB_yO_{2-δ} (A, B = Zr, Pr and/or La; 0 ≤ x, y ≤ 0.1). Supported by ICP analysis quantification, this study proposes an overview of the influences of residence time, temperature and precursors' concentration over the proportion of the substitution element in the CeO₂ NCs. This work demonstrates a fast and simple process to Ce_{1-x-y}A_xB_yO_{2-δ} nanostructures synthesis using scH₂O synthesis.

Keywords : Cerium oxide, Nanoparticles, Supercritical fluids, Continuous process, Substitution

1. Introduction

Over the past decades, cerium oxide based materials (pure or substituted) have been intensively studied as they have been proven to be effective materials in a wide range of applications including catalysis, oxygen storage, polishing, optics or biomedicine [1-7]. In particular, substituted CeO₂ (substitution of Ce atoms by other elements with lower oxidation state, typically +II or +III) is used to control oxygen vacancies within the oxide structures, which can greatly enhance the material properties. Several examples of substituted ceria have been reported with various atoms including La, Pr, Zr, Al or Cu [8-10].

Most of the applications seek for synthesis processes displaying high reproducibility and advanced control over the materials characteristics, physicochemical properties and composition. Historically, homogeneous precipitation based methods remain the most reported approaches for the synthesis of cerium oxide-based materials as they are today mastered, cheap and easily operated [11-14], [9]. However, the involved chemical reactions are slow-paced and the control over materials properties is limited [15-16].

In order to address these limitations, alternative synthesis methods have been studied (colloidal approaches, solvothermal reactions, use of solvents with high boiling point, etc.) [17-20]. Among them, near- and supercritical fluids mediated reactions have demonstrated their efficiency for the synthesis of cerium oxide particles with tailor-made properties (size, shape, surface chemistry, etc.) [21-23]. Several works have investigated the influence of experimental parameters (temperature, precursor, solvent, residence time, etc.) for the control of synthesized materials properties [24-26]. Furthermore, CeO₂ nanoparticles synthesis in near- and supercritical fluids can be continuously processed in short time (less than 1 min), making them easily scalable [27].

However, only few publications report on the substitution of Ce atoms by other elements in CeO_2 (e.g. $\text{Ce}_{1-x}\text{A}_x\text{O}_{2-\delta}$, $0 \leq x \leq 1$) via continuous supercritical fluids techniques and $\text{Ce}_{1-x}\text{Zr}_x\text{O}_{2-\delta}$ remains the only studied system in such conditions. For instance, Cabañas et al. proposed a quantification of elements in $\text{CeO}_2\text{-ZrO}_2$ mixed oxides synthesized in $n\text{CH}_2\text{O}$ ($T = 300\text{ }^\circ\text{C}$ and $p = 25\text{ MPa}$) from zirconium acetylacetonate and cerium ammonium nitrate. These analyses revealed small difference between initial precursor concentrations and Ce:Zr ratios in the final powders [28-29]. Kim et al. also reported the continuous synthesis of $\text{CeO}_2\text{-ZrO}_2$ mixed oxides in supercritical H_2O^1 (sCH_2O) at $T = 400\text{ }^\circ\text{C}$ and $p > p_c$, from cerium nitrate and zirconium oxynitrate [30-32]. A three injection lines process was used and pH was controlled thanks to an ammonia solution. Similarly, zirconium acetylacetonate coupled with cerium ammonium nitrate was used by Trysted et al. for the *in situ* synchrotron study of the batch mode mixed oxides synthesis in sCH_2O ($T = 375\text{ }^\circ\text{C}$ and $p = 23\text{ MPa}$) [33]. Note that whatever the synthesis approach, it is known that for small substitution percentage (<30%), substituted cerium oxide materials keep the pure cerium oxide crystalline structure and morphology [33].

Based on the above-mentioned considerations, this study first deals with the continuous synthesis of pure CeO_2 in near- and supercritical conditions from two different precursors (cerium nitrate and cerium ammonium nitrate) in water. Starting from the experimental analyses and theoretical statements, we propose reaction mechanisms to highlight the influence of experimental parameters over the physicochemical characteristics of the synthesized materials. Then, the synthesis of substituted cerium oxide nanoparticles is investigated thanks to those preliminary results. Aiming at broadening the range of elements conceivable for the synthesis of substituted cerium oxide in near- and supercritical fluids, three different elements are considered: lanthanum, praseodymium and zirconium. Experiments were performed to quantify the influences of the precursor's reactivity, the residence time and the temperature over the final substitution rate. Based on the obtained results, protocols are proposed to synthesize lanthanum, praseodymium and/or zirconium substituted CeO_2 nanoparticles with controlled compositions.

2. Experimental

2.1. Chemicals

Cerium(III) nitrate (purity: 99%), ammonium cerium(IV) nitrate (purity $\geq 98.5\%$), zirconium(IV) oxynitrate (purity: 99%), lanthanum(III) nitrate (purity: 99.99%) and praseodymium nitrate (purity: 99.9%) were purchased from Sigma Aldrich and used as received.

2.2. Apparatus and procedure

The cerium oxide based nanostructures have been synthesized using a simple custom-built, continuous-flow reactor, presented in Fig. 1 [26], [34].

The feed-tank was a 500 mL Pyrex beaker containing the precursor(s) and the solvent(s) under fast magnetic stirring. The reactor was made of 1/8 in. 316 L stainless steel coiled tubing with an internal diameter of 1.57 mm, for a total volume of 8 cm^3 . The heater was a homemade coiled ceramic resistance controlling the temperature up to $500 \pm 1\text{ }^\circ\text{C}$. The high-pressure pump (P) was a controlled flow pump (JASCO PU2080), delivering flow rates up to $10 \pm 0.001\text{ mL min}^{-1}$. A back pressure regulator (BPR – JASCO BP 2080), placed downstream the reactor, allows controlling the pressure in the reactor up to $40 \pm 0.1\text{ MPa}$. In this process, the precursors (cerium precursor alone or along with the substituting agent precursor) are directly mixed with the solvent(s) before being injected inside the reactor with the high pressure pump, via a single injection line, while classical methods imply two or more separate lines for precursors and solvents [24], [35].

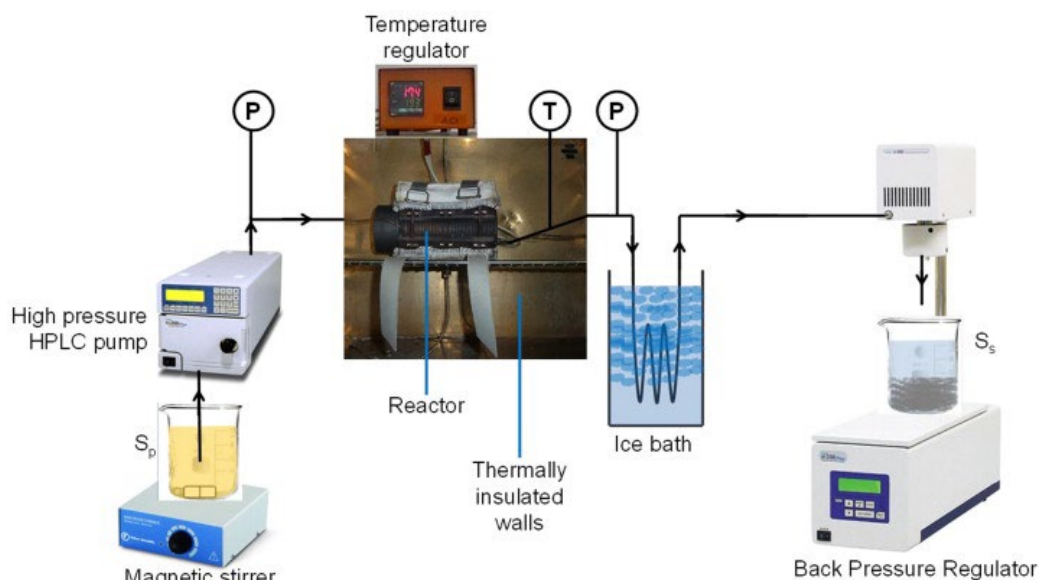


Fig. 1. Custom-built continuous process for CeO_2 synthesis in supercritical media. T = thermocouple; P = manometer; S_p = precursor solution and S_s = synthesis solution (synthesized powders + solvent).

The mixture is then flown through the reactor at near- or supercritical conditions, where the nucleation/growth of nanostructures occurs. The reaction is quenched thermally downstream the reactor with an ice bath, and the NCs can be recovered in solution upon depressurization through the BPR. The solution is then filtered and the synthesized materials are washed on a Büchner filter system. The dry powders have been then analyzed without any annealing treatment.

2.3. Synthesis of cerium oxide-based powders

As previously mentioned, two kinds of systems were investigated: (i) pure CeO_2 from two different precursors and (ii) $\text{Ce}_{1-x-y}\text{A}_x\text{B}_y\text{O}_{2-\delta}$ NCs with three different substitution elements – A, B = Zr, Pr and/or La; $0 \leq x, y \leq 0.1$.

2.3.1. Pure cerium oxide nanostructures

Two experiments have been performed in order to determine the influence of the starting cerium precursor (cerium nitrate or ammonium cerium nitrate) on cerium oxide synthesis in supercritical water conditions, in particular over the processability and the obtained nanostructures morphologies. Both precursors were dispersible in water. For scH_2O experiments, the conditions were set at $T = 400^\circ\text{C}$ and $p = 24.5\text{ MPa}$. The precursor concentration was fixed at 10^{-2} M in all cases.

2.3.2. Zirconium, lanthanum and praseodymium substituted cerium oxide nanostructures

Concerning the substitution studies, eighteen screening experiments have been first performed in order to determine the influence of temperature and residence time. The precursors' solutions were composed of an aqueous mixture of ammonium cerium nitrate ($9 \times 10^{-3}\text{ M}$) and hydrated substituting elements' precursors ($1 \times 10^{-3}\text{ M}$ zirconium oxynitrate, lanthanum nitrate or praseodymium nitrate). Two temperatures have been chosen: 300°C (ncH_2O) and 400°C (scH_2O), while residence time (R_t) was tuned in the range 10–60 s. Operating pressure has been fixed at 24.5 MPa. In a second time, six experiments were performed in scH_2O in order to synthesize cerium oxide based nanostructures ($\text{Ce}_{1-x}\text{A}_x\text{O}_{2-\delta}$) with controlled compositions (A = La, Pr, Zr or mixtures, $0 < x < 0.1$). Based on the previous screening experiments, the operating conditions were fixed at $T = 400^\circ\text{C}$ $p = 24.5\text{ MPa}$ and $R_t = 10\text{ s}$. The substituting elements' precursors remain the same as above-mentioned as well as the ammonium cerium nitrate concentration ($9 \times 10^{-3}\text{ M}$); however, their concentrations have been adjusted depending on the targeted substitution rate.

2.4. Characterization techniques

The XRD patterns were recorded on a PANalytical X'Pert MPD powder diffractometer (θ - θ Bragg-Brentano geometry using Cu $K_{\alpha 1, \alpha 2}$ ($\lambda_1 = 1.54060 \text{ \AA}$, $\lambda_2 = 1.54441 \text{ \AA}$) radiation, equipped with a secondary monochromator and a X'Celerator detector, in the range of 8 – 120° , in continuous scan mode at $3.5 \times 10^{-3} \text{ s}^{-1}$. The powder was ground and sieved at 50 \mu m before being analyzed by XRD. The TEM images were obtained using a Hitachi H7650 transmission electron microscope operated at 90 kV . Samples were prepared by depositing drops of toluene or ethanol dispersed samples on copper-carbon grids.

The FTIR measurements were carried out using a Bruker Equinox 55 spectrophotometer. The spectra were recorded over 32 scans in the range of 400 – 4000 cm^{-1} , with a resolution of 4 cm^{-1} , using KBr powder technique.

Inductively coupled plasma (ICP) atomic emission spectroscopy was systematically used on doped powders in order to quantify elements in the synthesized materials. Measurements were realized using a Varian 720-ES emission spectrometer.

Chemical cartography of the elements in the substituted powders was obtained using a JEOL 2200 FX scanning transmission electron microscope (STEM) coupled with an energy-dispersive X-ray (EDX) spectrometer.

3. Results and discussions

3.1. Processing of pure cerium oxide nanostructures: influence of precursors

3.1.1. Processability and materials characterization

Experiments have been carried out in order to identify the precursor enabling the continuous synthesis of CeO_2 in water using our single-line process.

The experiment performed in scH_2O from ammonium cerium nitrate has allowed a continuous recovery of materials, leading to well crystallized CeO_2 (crystallinity above 95%, evaluated from the internal standard method), in a fcc system with lattice parameters of $5.41 \pm 0.005 \text{ \AA}$, calculated from the XRD data using Bragg's equation (Fig. 2). Oppositely, the experiment conducted in scH_2O from cerium nitrate has led to the precipitation of synthesized materials into the reactor.

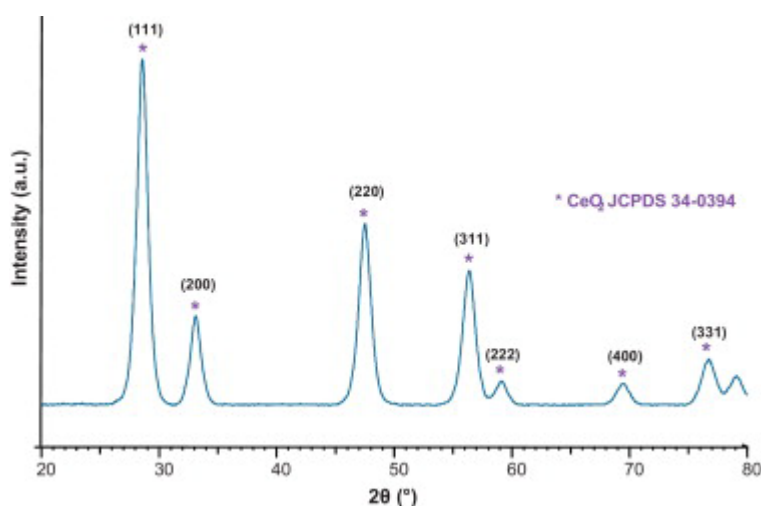


Fig. 2. XRD patterns of CeO_2 powder recovered continuously from the synthesis in scH_2O from ammonium cerium nitrate ($400 \text{ }^\circ\text{C}$; 24.5 MPa).

The material synthesized in scH_2O from cerium ammonium nitrate has been further examined by transmission electron microscopy (TEM) showing little aggregated CeO_2 NCs (5 – 10 nm) (Fig. 3a).

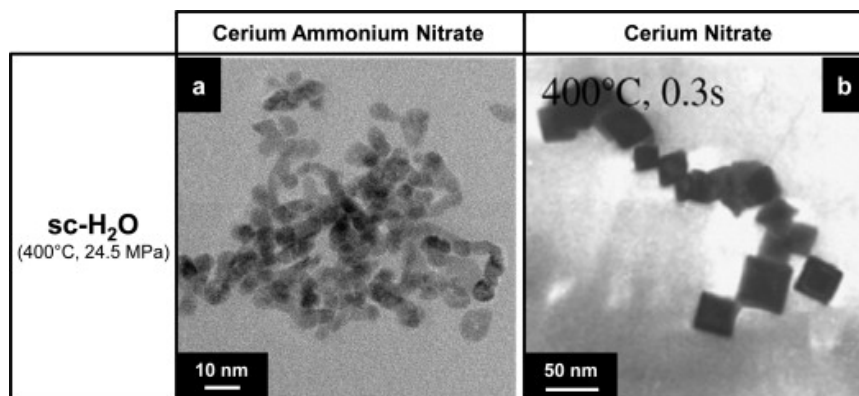


Fig. 3. TEM images of powders synthesized in SCFs: (a) CeO_2 NCs from ammonium cerium nitrate in scH_2O and (b) CeO_2 octahedrons from cerium nitrate in scH_2O (adapted from [36]).

Please note that our single injection line process did not allow the continuous powders recovery when cerium nitrate is used as precursor in scH_2O . However, it is worth mentioning that a two injection line process mixing the precursor solution with pre-heated supercritical water flow, developed by Adschiri et al. was previously successfully used to obtain small (20–40 nm) CeO_2 octahedrons in similar conditions (Fig. 3b) [21], [36]. We believe that our lower flow rates and the single injection line process are responsible for the precipitation of the particles during synthesis, oppositely to the experiments led by Hakuta et al. or Veriansyah et al. [21], [24].

3.1.2. Proposed mechanisms

The obtained results, along with those presented in our previous work [26], have shown the flexibility of supercritical media for the synthesis of well-crystallized CeO_2 nanostructures with various sizes and morphologies. To date, the mechanisms associated with the formation of CeO_2 in supercritical water remains partially elucidated.

The hydrothermal transformations involved during the synthesis in scH_2O are highly influenced by the nature of the precursor (counter-ions – such as NO_3^- or NH_4^+ – and initial oxidation state of cerium). Mechanisms involved in hydrothermal synthesis of CeO_2 and, *a fortiori*, in scH_2O go through the formation of a cerium hydroxide (+III or +IV), which will be oxidized (if starting oxidation state is +III) and dehydrated to obtain the cerium oxide (+IV) [11], [37–38]. Two kinds of morphologies (polyhedrons and NCs) can be observed depending on the considered precursor. Considering the syntheses from cerium nitrate in scH_2O , the nitrate counter-ions can play the role of an oxidizing agent leading to the recovery of pure CeO_2 only. Furthermore, polyhedron morphology, also observed by Hakuta et al. [21], can be explained by the selective adsorption of nitrate anions on the surface of CeO_2 nuclei leading to an anisotropic growth of the particles to obtain cubes or polyhedrons as evidenced by Wu et al. [39].

Regarding the synthesis from ammonium cerium nitrate in scH_2O , CeO_2 NCs are continuously recovered with our single-line injection process. The NCs exhibit morphologies, which have been also obtained by Mai et al. *via* the hydrothermal synthesis of cerium oxide from ammonium cerium nitrate [40]. They postulated that the oxidation state of the cerium precursor was the unique factor governing the morphology: Ce^{4+} ions contributing to a fast formation of CeO_2 nuclei, less soluble and less anisotropic than $\text{Ce}(\text{OH})_3$ intermediate species, resulting in the formation of nanoparticles instead of nanocubes. Although the oxidation state of the precursor may be of key importance for reaction pathways and kinetics, the influence of ammonium cations cannot be discarded.

In order to confirm the role of NH_4^+ cations, we have conducted a synthesis in scH_2O (300 °C; 24.5 MPa) from an equimolar mixture of cerium nitrate and ammonium cerium nitrate. This experiment led to the continuous synthesis (no precipitation in the reactor) of well-crystallized CeO_2 NCs of 5–10 nm, while no cubes were observed. The mixture of the two precursors induces the equimolar presence of Ce^{3+} and Ce^{4+} in the reaction media (Ce^{3+} to Ce^{4+} oxidation being ensured by NO_3^-

anions). Thus, the sole formation of NCs, instead of a potential expected mixture of NCs and nanocubes, proves that the oxidation state of the precursor has no influence on the morphology unlike the NH_4^+ cations.

Based on these results, we proposed that during the synthesis of CeO_2 from $\text{Ce}(\text{NO}_3)_6(\text{NH}_4)_2$ in scH_2O , NO_3^- anions adsorb on the surface of CeO_2 similarly to the synthesis from $\text{Ce}(\text{NO}_3)_3$ in scH_2O . However, the $\text{p}K_w$ of scH_2O being high at 400 °C and 24.5 MPa ($\text{p}K_w = 19.4$), the NCs are not stabilized, explaining the precipitation of CeO_2 synthesized from $\text{Ce}(\text{NO}_3)_3$ in our single line process. Oppositely, the NH_4^+ anions present during the syntheses from $\text{Ce}(\text{NO}_3)_6(\text{NH}_4)_2$ may act as electrostatic stabilizers for the $(\text{CeO}_2\text{--NO}_3)$ system, avoiding the precipitation of the particles and therefore allowing the continuously recovery of small CeO_2 NCs.

The presence of NO_3^- anions at the surface of cerium oxide synthesized in water has been evidenced thanks to an experiment performed in ncH_2O (300 °C and 24.5 MPa) from $(\text{NH}_4)_2\text{Ce}(\text{NO}_3)_6$. IR spectra of the recovered CeO_2 NCs shows a band at 1383 cm^{-1} , which can be attributed to the vibration band of free NO_3^- in KBr (Fig. 4), while no band was detected for CeO_2 NCs synthesized from $(\text{NH}_4)_2\text{Ce}(\text{NO}_3)_6$ in scEtOH [26].

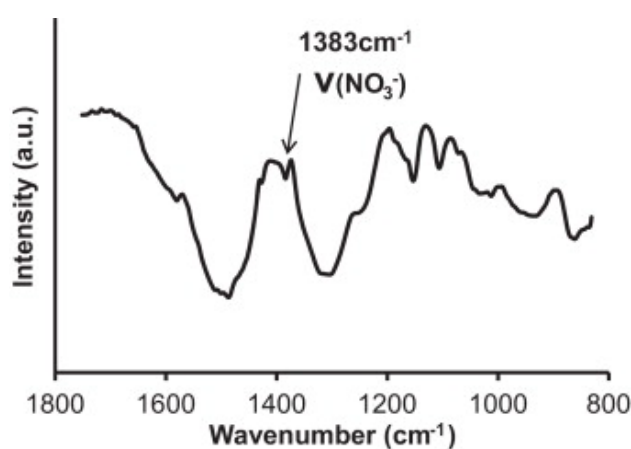


Fig. 4. Transmission FTIR spectra of CeO_2 nanoparticles synthesized at 300 °C and 24.5 MPa in water ($t_s = 45$ s) from cerium ammonium nitrate. The spectrum has been recorded on as synthesized powders.

Based on this preliminary study concerning pure CeO_2 NCs synthesis in near- and supercritical fluids, we have investigated in a second part the substitution of Ce by La, Pr and Zr atoms in CeO_2 NCs with such processes.

3.2. Synthesis of $\text{Ce}_{1-x}\text{A}_x\text{O}_{2-\delta}$ (A = La, Pr, Zr) nanostructures in near- and supercritical water

In order to study the suitability and the efficiency of supercritical media for the synthesis of substituted cerium oxide materials, we have chosen to select cerium ammonium nitrate as cerium precursor as it leads to dispersed nanoparticles and enable continuous recovery of the materials with our process, oppositely to cerium nitrate.

In order to limit the influence of the substitution element precursor, we also chose to select them so that they are as close as possible to the cerium precursor, *i.e.* the cerium ammonium nitrate. As ammonium nitrate precursors were not available for the selected substitution elements, we purchased nitrate or oxynitrate precursors, assuming these counter-ions – coupled with cerium ammonium nitrate – will not affect noticeably the chemical reaction. Indeed, we have shown in Section 3.1 that a mixture of cerium ammonium nitrate with cerium nitrate leads to the same results (particles size, crystallinity, shape) as in the case of pure cerium ammonium nitrate.

3.2.1. Preliminary substitution experiments in near- and supercritical water

Screening experiments have been performed in order to determine the influence of temperature and residence time on the processing of zirconium, lanthanum and praseodymium substituted CeO_2 NCs. For each experiment, materials have been

recovered continuously without precipitation within the reactor. Powders have been analyzed as synthesized, without further calcination treatment. These 18 experiments have led to well crystallized NCs adopting the CeO₂ structure (crystallinity above 95%, evaluated from the internal standard method), in a fcc system with lattice parameters of $5.41 \pm 0.005 \text{ \AA}$ (obtained in all cases with no detectable variations), calculated from the XRD data using Bragg's equation (Fig. 5). All powders displayed crystallite sizes inferior to 10 nm according to Scherrer's equation, whatever the considered operating parameters.

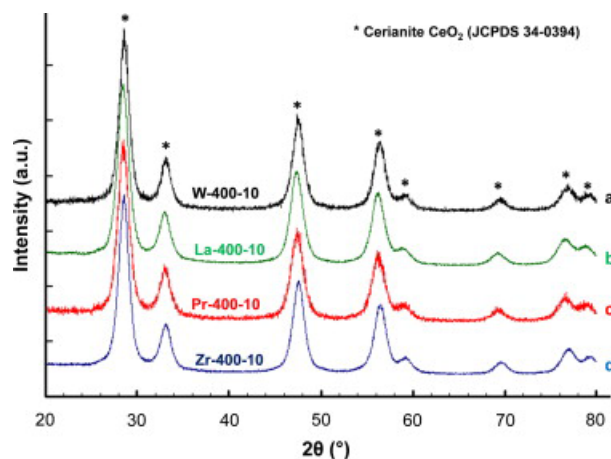


Fig. 5. XRD patterns of materials synthesized in sch_2O at 400 °C and 24.5 MPa for a residence time of 10 s from ammonium cerium nitrate (a) alone, (b) with 10% of lanthanum nitrate, (c) with 10% of praseodymium nitrate and (d) with 10% of zirconium oxynitrate.

The focus of these screening experiments being to determine the influence of temperature and residence time on the substitution process efficiency, ICP analyses have been carried out on each material. Results of these analyses are given in Table 1. Well crystallized substituted CeO₂ NCs are obtained with a molar composition of 7.4%, 2.8% and 5.2% for Zr, La and Pr, respectively, starting from an initial 10% molar concentration of the substituting element precursor. The results show that for the three selected precursors, residence time has no influence on substitution efficiency after 10 s, which means that reaction is fast for all precursors independently from the operating temperature. However, higher temperatures appear to enhance the reactivity of the lanthanum and praseodymium precursors, while no influence is noticed for the reactivity of the zirconium precursor.

Table 1
Operating conditions of the screening tests and percentage of substitution (x) of Ce by the substituting element in the recovered materials, determined by ICP analysis. Screening experiments have been performed in water for a pressure of 24.5 MPa.

Substitution atom	Temperature (°C)	R_t (s)	x (mol %)
Zr	300	45	7.3
		60	7.3
		10	7.4
	400	30	7.2
		45	7.3
		60	7.2
La	300	45	0.9
		60	1.0
		10	2.8
	400	30	2.4
		45	2.6
		60	2.5
Pr	300	45	2.4
		60	2.5
		10	5.2
	400	30	4.2
		45	4.3
		60	4.8

3.2.2. Preparation of cerium based nanostructures with controlled composition

The above-mentioned screening experiments show the limits of the reactivity of the substitution element precursors for the synthesis of $\text{Ce}_{1-x}\text{A}_x\text{O}_{2-\delta}$ NCs with controlled composition in supercritical water. TGA analyses have been conducted on lanthanum nitrate, praseodymium nitrate and zirconium oxynitrate precursors (Fig. 6). Two conclusions arise from these analyses. First, whatever the considered precursor, the thermal decomposition is not fully achieved at 400 °C, unlike the thermal decomposition of ammonium cerium nitrate to cerium oxide is achieved at 230–240 °C according to Zhou et al. [41]. Note that hydrothermal processes will not necessarily reach equivalent transformation temperatures as for thermal processes, given the different mechanisms involved; however, we assumed that the tendency should remain similar in both cases.

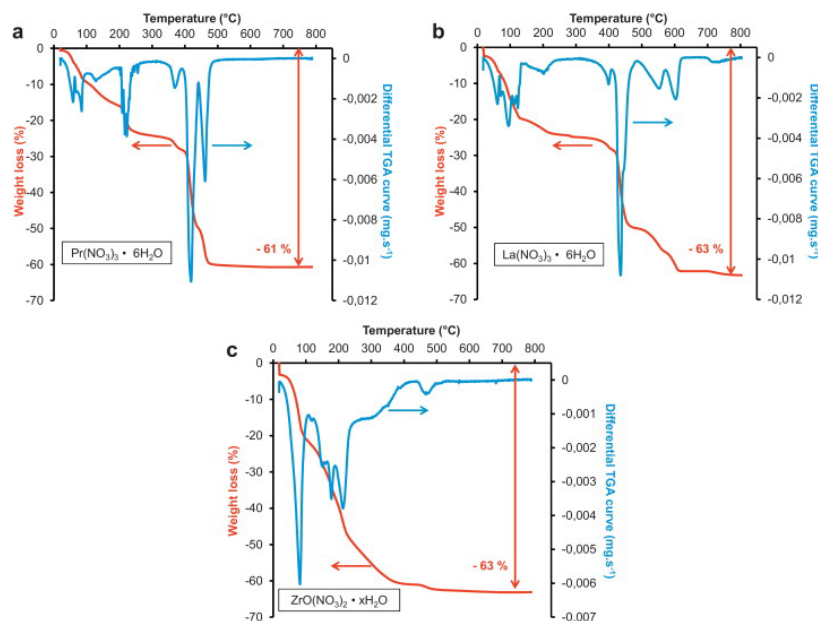


Fig. 6. TGA curves of (a) praseodymium nitrate hexahydrate, (b) lanthanum nitrate hexahydrate and (c) zirconium oxynitrate hydrate. Analyses have been conducted under N_2 with a heating rate of $2\text{ }^\circ\text{C min}^{-1}$.

The second information is that the decomposition rate (=weight loss at T /total weight loss) as a function of temperature is not the same depending on the considered precursor. For instance, at 400 °C, the decomposition rate is 57%, 41% and 97% for praseodymium nitrate, lanthanum nitrate and zirconium oxynitrate, respectively, reflecting a different reactivity of each precursor.

According to all these results, two solutions can be considered in order to enhance/control the amount of substituting element into the CeO_2 NCs in a range typically interesting for most of the considered applications (e.g. $x < 0.1$): increase the temperature to enhance the reactivity of the precursors or use higher concentration in the substituting element starting solution.

In this work, we considered an increase of the substituting element solution concentration, while keeping the same cerium precursor concentration (9×10^{-3} M), in order to reach higher substitution rate. Six additional experiments have been performed at 400 °C, 24.5 MPa and $R_t = 10$ s) to produce substituted and double substituted CeO_2 NCs with different compositions. Once again, materials have been recovered continuously and crystallinity of materials (adopting CeO_2 structure) has been checked by XRD analyses. Substituting element(s) percentages in the precursor solution and in the recovered materials (ICP analyses) are given in Table 2. These results show that it is possible to synthesize in sCH_2O substituted cerium oxide NCs with controlled Ce substitution rates by tuning the concentration of substituting element precursors. Using that technique, we were able to elaborate $\text{Ce}_{1-x-y}\text{A}_x\text{B}_y\text{O}_{2-\delta}$ with A and/or B = lanthanum, praseodymium or zirconium.

Table 2Composition of the substituted CeO₂ NCs synthesized in scH₂O (400 °C, 24.5 MPa and $R_t = 10$ s) using an extra amount of substituting element(s).

Mol% in precursor solution			Mol% in substituted CeO ₂ NCs ^a			Sample designation	d_{TEM}^b (nm)
Pr	La	Zr	Pr	La	Zr		
10.1			5.2			Ce _{0.95} Pr _{0.05} O _{2-δ}	6.9 ± 1.4
30.8			8.2			Ce _{0.92} Pr _{0.08} O _{2-δ}	6.8 ± 1.2
	30.8			4.0		Ce _{0.96} La _{0.04} O _{2-δ}	6.0 ± 0.9
		14.3			9.5	Ce _{0.91} Zr _{0.09} O ₂	7.7 ± 2.0
8.3	16.7		3.7	1.7		Ce _{0.94} La _{0.02} Pr _{0.04} O _{2-δ}	6.6 ± 1.1
9.3		7.0	4.6		5.0	Ce _{0.90} Zr _{0.05} Pr _{0.05} O _{2-δ}	7.5 ± 1.3

^a Determined by ICP.^b Particles sizes (d_{TEM}) have been analyzed using the ImageJ software by counting over 100 particles.

Size and size distribution of the synthesized substituted nanoparticles were analyzed by TEM, showing that the obtained substituted CeO₂ NCs keep the same morphology displayed by pure cerium oxide NCs synthesized in the same conditions, *i.e.* narrow size distributed and slightly aggregated nanocrystals (Fig. 7).

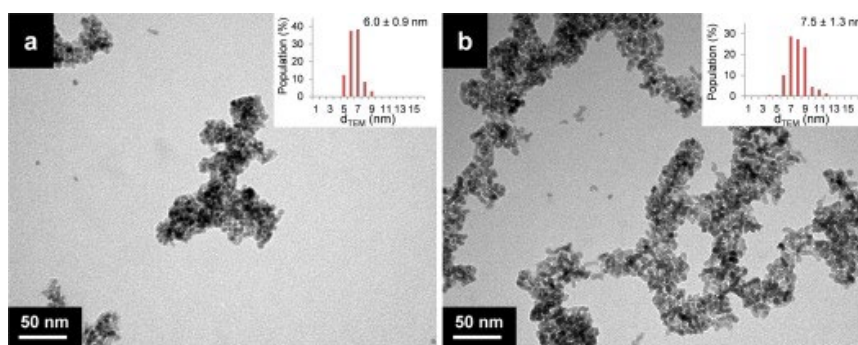


Fig. 7. TEM images of the samples. (a) Ce_{0.96}La_{0.04}O_{2-δ} and (b) Ce_{0.90}Zr_{0.05}Pr_{0.05}O_{2-δ}. The powders were dispersed in ethanol for microscopy sample preparation.

Additionally, the sizes calculated from TEM images are coherent with crystallite sizes calculated from XRD ($d_{\text{TEM}} \approx d_{\text{cr}}$) patterns, meaning the nanoparticles are single nanocrystals (Table 2).

Finally, STEM-EDX analyses have been conducted for checking the substitution homogeneity over the synthesized materials. Chemical cartography of the elements clearly shows that all elements are equally distributed in the NCs, resulting in homogenous substituted cerium oxide nanostructures (Fig. 8).

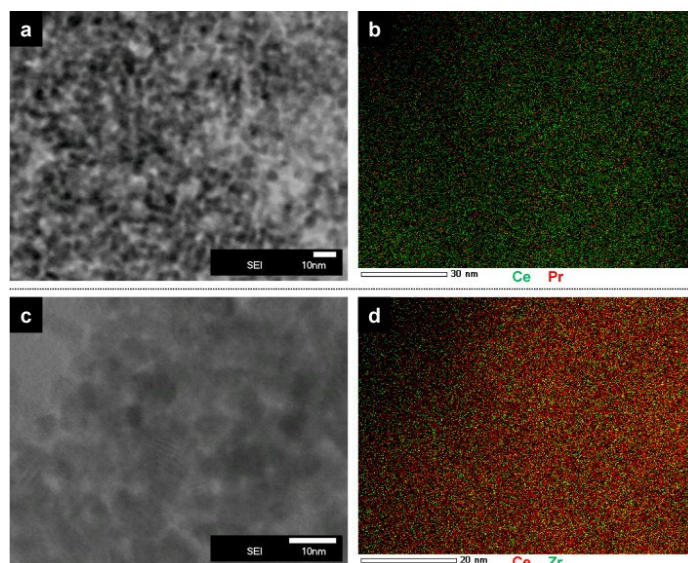


Fig. 8. SEM images and chemical cartographies of the samples (a and b) Ce_{0.95}Pr_{0.05}O_{2-δ} and (c and d) Ce_{0.91}Zr_{0.09}O₂. The powders were dispersed in ethanol for microscopy sample preparation.

3.2.3. Discussion

To the best of our knowledge, these experiments are the first reporting the synthesis of CeO₂ NCs substituted with lanthanum and praseodymium using a continuous supercritical water process. Zirconium substituted CeO₂ synthesis has already been reported in scH₂O using zirconium oxynitrate (without quantitative analysis of the elements repartition) or zirconium acetylacetonate (XRF analyses showing small difference between initial and final Ce:Zr ratios) [28-29].

Our study has demonstrated the suitability of the near- and supercritical water synthesis processes to obtain substituted CeO₂ nanostructures. Although chemical cartographies showed a homogeneous repartition of the elements in the obtained materials, quantitative analyses performed by ICP displayed differences between initial and final elements ratios and evidenced the importance of some experimental parameters. Indeed, reactivity of the precursors is of key importance in order to synthesize such materials. This reactivity is directly linked to the precursor itself (counter-ion/ligand and oxidation state) but also to the experimental conditions (T and p) and the time of reaction (t_s). The real challenge is therefore to find suitable precursors for each element with similar reactivity.

Temperature appears to have a real influence when considering lanthanum and praseodymium nitrates. Indeed, a higher reactivity of these precursors has been observed at 400 °C compared to 300 °C, leading to higher substitution rates in the synthesized substituted CeO₂ materials. Higher experimental temperature ($T > 500$ °C, *i.e.* above the thermal decomposition temperature of the precursors) should allow reaching higher reactivity of these precursors but with a risk to form a secondary oxide phase from the substitution element. Such temperatures would be coherent with those generally reported for the synthesis of lanthanum or praseodymium substituted CeO₂ *via* usual methods [42-45]. However, it has to be noticed that such conditions could compromise CeO₂ NCs characteristics [46].

In contrast, temperature appears to have little effect when starting from zirconium oxynitrate. The maximal reactivity of this precursor is possibly already reached at 300 °C, which is coherent with the syntheses led by Kim et al. in scH₂O (400 °C; $p > p_c$) [30-32].

Finally, these experiments showed no noticeable effect of the residence time above 10 s, whatever the considered precursor.

Looking upon such considerations, we were able to synthesize CeO₂-based NCs (7 nm) with narrow size distribution, controlled substitution rates and homogeneous dispersion of the elements by playing on initial precursors ratios. Such materials can be synthesized continuously in much shorter residence times than the conventional techniques (co-precipitation).

4. Conclusion

The influence of two cerium precursors (nitrate or ammonium nitrate) has been investigated for the synthesis of pure CeO₂ using a simple continuous process in scH₂O. The cerium nitrate in scH₂O system led to the precipitation of the CeO₂ within the reactor, which is not the case with cerium ammonium nitrate allowing a continuous recovery of CeO₂ nanoparticles (size of about 7 nm). Based on experimental analyses and literature results, we have proposed reaction mechanisms to explain the observed behavior. In scH₂O (400 °C; 24.5 MPa), the counter-ion of the cerium precursor has the most important influence, the counter-ion playing both the role of an oxidizer (the nitrate ions allowing the transition from Ce³⁺ to Ce⁴⁺) and a stabilizing agent. Indeed, nitrate anions orientate the growth of CeO₂ nuclei, while ammonium cations stabilize the [nitrate–CeO₂] systems. That way, materials synthesized from cerium ammonium nitrate in scH₂O will be stabilized in the solvent by ammonium ions and lead to continuous recovery of well-dispersed NCs.

Then, the [cerium ammonium nitrate/H₂O] system has been selected in order to perform substituting experiments of the CeO₂ NCs. XRD and TEM analyses have shown that substituted CeO₂ materials synthesized in near- or supercritical water

displayed the same morphology (nanoparticles), sizes (7 nm) and crystallinity (fcc) than pure CeO₂ NCs synthesized in the same conditions. Furthermore, ICP and STEM-EDX analyses evidenced a homogeneous distribution of the substituting elements in the obtained materials with a substitution rate depending on experimental conditions (precursor, T and R_t). Thus, these experiments have shown that a temperature of 300 °C is sufficient enough to get an almost maximum reactivity with zirconium oxynitrate, while temperature above 400 °C are required to fully complete lanthanum nitrate and praseodymium nitrate transformation. The obtained results also demonstrated that above 10 s, residence time has no more influence on the reactivity of the precursors, meaning that such syntheses could be conducted in less than 10 s at supercritical conditions, while hours are generally needed through co-precipitation methods. The synthesis of Ce_{1-x}A_xO_{2-δ} and Ce_{1-x-y}A_xB_yO_{2-δ} NCs with controlled composition was successfully achieved through this process using an excess of substitution element precursor in the starting precursor solution to overcome the difference in reactivity of the precursors.

Such results and observations allow a better understanding of the influence of the experimental parameters for the synthesis of CeO₂ based materials in solvothermal conditions and evidence the necessity of precursors with similar reactivity.

Acknowledgments

The authors acknowledge the financial support of the "Région Aquitaine" and the help of the Bordeaux Imaging Center (BIC) for the electronic microscopy characterization.

References

1. W. Hernandez, O. Laguna, M. Centeno, J. Odriozola. **Structural and catalytic properties of lanthanide (La, Eu, Gd) doped ceria.** Journal of Solid State Chemistry, 184 (2011), pp. 3014-3020.
2. S. Meher, G. Ranga Rao. **Tuning, via counter anions, the morphology and catalytic activity of CeO₂ prepared under mild conditions.** Journal of Colloid and Interface Science, 373 (2012), pp. 46-56.
3. H. Yao, Y. Yao. **Ceria in automotive exhaust catalysts. I. Oxygen storage.** Journal of Catalysis, 86 (1984), pp. 254-265.
4. S. Abdollahzadeh-Ghom, C. Zamani, T. Andreu, M. Epifani, J. Morante. **Improvement of oxygen storage capacity using mesoporous ceria-zirconia solid solutions.** Applied Catalysis B: Environmental, 108-109 (2011), pp. 32-38.
5. C. Stanek, A. Tan, S. Owens, R. Grimes. **Atomistic simulation of CeO₂ surface hydroxylation: implications for glass polishing.** Journal of Materials Science, 43 (2008), pp. 4157-4162.
6. J.-H. Cho, M. Bass, S. Babu, J. Dowding, W. Self, S. Seal. **Up conversion luminescence of Yb³⁺Er³⁺ codoped CeO₂ nanocrystals with imaging applications.** Journal of Luminescence, 132 (2012), pp. 743-749.
7. G. Renu, V. Divya Rani, S. Nair, K. Subramanian, V.-K. Lakshmanan. **Development of cerium oxide nanoparticles and its cytotoxicity in prostate cancer cells.** Advanced Science Letters, 6 (2012), pp. 17-25.
8. B. Reddy, A. Khan, Y. Yamada, T. Kobayashi, S. Loidant, J.-C. Volta. **Structural characterization of CeO₂-MO₂ (M = Si⁴⁺, Ti⁴⁺, and Zr⁴⁺) mixed oxides by Raman spectroscopy, X-ray photoelectron spectroscopy, and other techniques.** Journal of Physical Chemistry B, 107 (2003), pp. 11475-11484.
9. S. Bishop, T. Stefanik, H. Tuller. **Defects and transport in Pr_xCe_{1-x}O_{2-δ}: composition trends.** Journal of Materials Research, 27 (2012), pp. 2009-2016.
10. Uslu, A. Aytimur, M. Ozturk, S. Kocyigit. **Synthesis and characterization of neodymium doped ceria nanocrystalline ceramic structures.** Ceramics International, 38 (2012), pp. 4943-4951.
11. P.-L. Chen, I.-W. Chen. **Reactive cerium(IV) oxide powders by the homogeneous precipitation method.** Journal of the American Ceramic Society, 76 (1993), pp. 1577-1583.
12. X.-D. Zhou, W. Huebner, H. Anderson. **Room-temperature homogeneous nucleation synthesis and thermal stability of nanometer single crystal CeO₂.** Applied Physics Letters, 80 (2002), pp. 3814-3816.

13. A.S. Deshpande, N. Pinna, P. Beato, M. Antonietti, M. Niederberger. **Synthesis and characterization of stable and crystalline $Ce_{1-x}Zr_xO_2$ nanoparticle sols.** Chemistry of Materials, 16 (2004), pp. 2599-2604.
14. L. Sronek, J. Majimel, Y. Kihn, Y. Montardi, A. Tressaud, M. Feist, C. Legein, J.-Y. Buzare, M. Body, A. Demourgues. **New highly divided Ce–Ca-based oxyfluorides with UV-shielding properties: study of the $Ce_{1-x}Ca_xO_{2-x}$ and $Ce_{1-x}Ca_xO_{2-x-y/2}F_y$ series.** Chemistry of Materials, 19 (2007), pp. 5110-5121.
15. T. Sreeremya, A. Krishnan, S. Iyengar, S. Ghosh. **Ultra-thin cerium oxide nanostructures through a facile aqueous synthetic strategy.** Ceramics International, 38 (2012), pp. 3023-3028.
16. N. Renuka. **Structural characteristics of quantum-size ceria nano particles synthesized via simple ammonia precipitation.** Journal of Alloys and Compounds, 513 (2012), pp. 230-235.
17. D. Terribile, A. Trovarelli, J. Llorca, C. De Leitenburg, G. Dolcetti. **The synthesis and characterization of mesoporous high-surface area ceria prepared using a hybrid organic/inorganic route.** Journal of Catalysis, 178 (1998), pp. 299-308.
18. T. Masui, K. Fujiwara, K.-I. Machida, G.-Y. Adachi, T. Sakata, H. Mori. **Characterization of cerium(IV) oxide ultrafine particles prepared using reversed micelles.** Chemistry of Materials, 9 (1997), pp. 2197-2204.
19. S. Depner, K. Kort, C. Jaye, D. Fischer, S. Banerjee. **Nonhydrolytic synthesis and electronic structure of ligand-capped CeO_2 -delta and CeOCl nanocrystals.** Journal of Physical Chemistry C, 113 (2009), pp. 14126-14134.
20. M. Hirano, E. Kato. **The hydrothermal synthesis of ultrafine cerium(IV) oxide powders.** Journal of Materials Science Letters, 15 (1996), pp. 1249-1250.
21. Y. Hakuta, S. Onai, H. Terayama, T. Adschiri, K. Arai. **Production of ultra-fine ceria particles by hydrothermal synthesis under supercritical conditions.** Journal of Materials Science Letters, 17 (1998), pp. 1211-1213.
22. E. Lester, P. Blood, J. Denyer, D. Giddings, B. Azzopardi, M. Poliakoff. **Reaction engineering: the supercritical water hydrothermal synthesis of nano-particles.** Journal of Supercritical Fluids, 37 (2006), pp. 209-214.
23. J. Zhang, S. Ohara, M. Umetsu, T. Naka, Y. Hatakeyama, T. Adschiri. **Colloidal ceria nanocrystals: a tailor-made crystal morphology in supercritical water.** Advanced Materials, 19 (2007), pp. 203-206.
24. B. Veriansyah, H. Park, J.-D. Kim, B.K. Min, Y.H. Shin, Y.-W. Lee, J. Kim. **Characterization of surface-modified ceria oxide nanoparticles synthesized continuously in supercritical methanol.** Journal of Supercritical Fluids, 50 (2009), pp. 283-291.
25. M. Kim, H.-S. Lee, Y. Shin, K. Ahn, Y.-S. Youn, J. Kim, Y.-W. Lee. **Vegetable oil aided hydrothermal synthesis of cerium oxide nanocrystals.** Korean Journal of Chemical Engineering, 29 (2012), pp. 1289-1291.
26. C. Slostowski, S. Marre, O. Babot, T. Toupance, C. Aymonier. **Near- and supercritical alcohols as solvents and surface modifiers for the continuous synthesis of cerium oxide nanoparticles.** Langmuir, 28 (2012), pp. 16656-16663.
27. T. Adschiri, Y. Hakuta, K. Arai. **Hydrothermal synthesis of metal oxide fine particles at supercritical conditions.** Industrial and Engineering Chemistry Research, 39 (2000), pp. 4901-4907.
28. Cabañas, J. Darr, E. Lester, M. Poliakoff. **A continuous and clean one-step synthesis of nano-particulate $Ce_{1-x}Zr_xO_2$ solid solutions in near-critical water.** Chemical Communications, 11 (2000), pp. 901-902.
29. Cabañas, J. Darr, E. Lester, M. Poliakoff. **Continuous hydrothermal synthesis of inorganic materials in a near-critical water flow reactor; the one-step synthesis of nanoparticulate $Ce_{1-x}Zr_xO_2$ ($x = 0-1$) solid solutions.** Journal of Materials Chemistry, 11 (2001), pp. 561-568.
30. J.-R. Kim, W.-J. Myeong, S.-K. Ihm. **Characteristics in oxygen storage capacity of ceria–zirconia mixed oxides prepared by continuous hydrothermal synthesis in supercritical water.** Applied Catalysis B: Environmental, 71 (2007), pp. 57-63.
31. J.-R. Kim, W.-J. Myeong, S.-K. Ihm. **Characteristics of CeO_2 – ZrO_2 mixed oxide prepared by continuous hydrothermal synthesis in supercritical water as support of Rh catalyst for catalytic reduction of NO by CO.** Journal of Catalysis, 263 (2009), pp. 123-133.
32. J.-R. Kim, K.-Y. Lee, M.-J. Suh, S.-K. Ihm. **Ceria–zirconia mixed oxide prepared by continuous hydrothermal synthesis in supercritical water as catalyst support.** Catalysis Today, 185 (2012), pp. 25-34.

33. C. Tyrsted, J. Becker, P. Hald, M. Bremholm, J. Pedersen, J. Chevallier, Y. Cerenius, S. Iversen, B. Iversen. **In-situ synchrotron radiation study of formation and growth of crystalline $Ce_xZr_{1-x}O_2$ nanoparticles synthesized in supercritical water.** Chemistry of Materials, 22 (2010), pp. 1814-1820.
34. S. Desmoulins-Krawiec, C. Aymonier, A. Loppinet-Serani, F. Weill, S. Gorsse, J. Etourneau, F. Cansell. **Synthesis of nanostructured materials in supercritical ammonia: nitrides, metals and oxides.** Journal of Materials Chemistry, 14 (2004), pp. 228-232.
35. S. Takami, S. Ohara, T. Adschiri, Y. Wakayama, T. Chikyow. **Continuous synthesis of organic-inorganic hybridized cubic nanoassemblies of octahedral cerium oxide nanocrystals and hexanedioic acid.** Dalton Transactions, 40 (2008), pp. 5442-5446.
36. K. Byrappa, S. Ohara, T. Adschiri. **Nanoparticles synthesis using supercritical fluid technology-towards biomedical applications.** Advanced Drug Delivery Reviews, 60 (2008), pp. 299-327.
37. B. Djuricic, S. Pickering. **Nanostructured cerium oxide: preparation and properties of weakly agglomerated powders.** Journal of the European Ceramic Society, 19 (1999), pp. 1925-1934.
38. X.-D. Zhou, W. Huebner, H. Anderson. **Processing of nanometer-scale CeO_2 particles.** Chemistry of Materials, 15 (2003), pp. 378-382.
39. Q. Wu, F. Zhang, P. Xiao, H. Tao, X. Wang, Z. Hu, Y. Lu. **Great influence of anions for controllable synthesis of CeO_2 nanostructures: from nanorods to nanocubes.** Journal of Physical Chemistry C, 112 (2008), pp. 17076-17080.
40. H.-X. Mai, L.-D. Sun, Y.-W. Zhang, R. Si, W. Feng, H.-P. Zhang, H.-C. Liu, C.-H. Yan. **Shape selective synthesis and oxygen storage behavior of ceria nanopolyhedra, nanorods, and nanocubes.** Journal of Physical Chemistry B, 109 (2005), pp. 24380-24385.
41. H. Zhou, Y. Zhang, H. Mai, X. Sun, Q. Liu, W. Song, C. Yan. **Spontaneous organization of uniform CeO_2 nanoflowers by 3D oriented attachment in hot surfactant solutions monitored with an in situ electrical conductance technique.** Chemistry, 14 (2008), pp. 3380-3390.
42. B. Zhang, D. Li, X. Wang. **Catalytic performance of La-Ce-O mixed oxide for combustion of methane.** Catalysis Today, 158 (2010), pp. 348-353.
43. V. Sharma, K. Eberhardt, R. Sharma, J. Adams, P. Crozier. **A spray drying system for synthesis of rare-earth doped cerium oxide nanoparticles.** Chemical Physics Letters, 495 (2010), pp. 280-286.
44. S. Somacescu, V. Parvulescu, J. Calderon-Moreno, S.-H. Suh, P. Osiceanu, B.-L. Su. **Uniform nanoparticles building $Ce_{1-x}Pr_xO_{2-\delta}$ mesoarchitectures: structure, morphology, surface chemistry, and catalytic performance.** Journal of Nanoparticle Research, 14 (2012), pp. 1-17.
45. L. Katta, P. Sudarsanam, B. Malleshram, B. Reddy. **Preparation of silica supported ceria-lanthana solid solutions useful for synthesis of 4-methylpent-1-ene and dehydroacetic acid.** Catalysis Science & Technology, 2 (2012), pp. 995-1004.
46. J.M. Heintz, J.C. Bernier. **Synthesis and sintering properties of cerium oxide powders prepared from oxalate precursors.** Journal of Materials Science, 21 (1986), pp. 1569-1573.